Gold Nanoparticles

Deutsche Ausgabe: DOI: 10.1002/ange.201500838
Internationale Ausgabe: DOI: 10.1002/anie.201500838

DNA-Encoded Tuning of Geometric and Plasmonic Properties of Nanoparticles Growing from Gold Nanorod Seeds**

Tingjie Song, Longhua Tang, Li Huey Tan, Xiaojing Wang, Nitya Sai Reddy Satyavolu, Hang Xing, Zidong Wang, Jinghong Li, Haojun Liang, and Yi Lu**

Abstract: *Systematically controlling the morphology of nanoparticles, especially those growing from gold nanorod (AuNR) seeds, are underexplored; however, the AuNR and its related morphologies have shown promises in many applications. Herein we report the use of programmable DNA sequences to control AuNR overgrowth, resulting in gold nanoparticles varying from nanodumbbell to nanooctahedron, as well as shapes in between, with high yield and reproducibility. Kinetic studies revealed two representative pathways for the shape control evolving into distinct nanostructures. Furthermore, the geometric and plasmonic properties of the gold nanoparticles could be precisely controlled by adjusting the base compositions of DNA sequences or by introducing phosphorothioate modifications in the DNA. As a result, the surface plasmon resonance (SPR) peaks of the nanoparticles can be fine-tuned in a wide range, from visible to second near-infrared (NIR-II) region beyond 1000 nm.*

Noble-metal nanocrystals such as gold nanoparticles (AuNPs) display a number of fascinating physical and chemical properties. One of the most intriguing properties is the localized surface plasmon resonance (LSPR), which is a result of the collective oscillations of free electrons on a confined metallic particle surface resonating at a specific wavelength of light.[1] As a result, these nanocrystals have shown promise for various applications, including optics,[2] imaging,[3] solar energy conversion,[4] and catalysis.[5] A critical factor in their successful applications is the fine control of their sizes and shapes, as these properties determine their performance.

Anisotropic nanoparticles such as gold nanorods (AuNRs) have LSPR tunable in a wide range and have found applications in biosensing[6] and biotherapeutics.[7] Tremendous efforts have been devoted to tailoring the plasmonic properties of AuNRs by synthetically tuning their sizes and shapes, achieving a tunable plasmonic resonance in the region between 600 to 850 nm.[2] However, tuning the AuNR growth with longitudinal LSPR (L-LSPR) beyond 850 nm is still challenging.[8] Having a LSPR beyond 850 nm in the near-IR absorbance region makes them particularly suitable in biomedical applications owing to reduced photon absorption and scattering by tissues.[9] Numerous reports have been published to improve the yield and uniformity in AuNR synthesis,[10] as well as to control geometric architectures.[11] Among the reports, the fine control of AuNR overgrowth was achieved by adding different capping ligands, such as cetyltrimethylammoniumbromide (CTAB),[12] glutathione, or cysteine.[13] Despite the progress made, modulating the AuNR overgrowth using versatile capping ligands with the ability to tune the plasmonic properties covering a wide range of plasmonic properties is still underdeveloped. Few methods can readily control the geometric and related properties of nanoparticles growing from the AuNR seeds with uniform sizes and shapes and in high yield and reproducibility.

To fully explore the control AuNR overgrowth using capping ligands, we explore the use of DNA molecules as a class of capping ligands, because the DNA can be readily programmed into different sequences[14] and modified with either artificial nucleobases or other functional groups.[15] These features allow DNA molecules to conjugate to nanomaterials and subsequently control nanoscale assembly with high precision in response to chemical and biological stimuli.[16] However, the majority of the studies rely on conjugation of DNA after the nanomaterials have been synthesized and DNA plays no role in influencing the nanomaterials' morphology. Recently, we have explored the use of different DNA sequences as programmable capping ligands to control nanoparticle morphologies.[17] The mechanisms of these DNA-mediated growth of gold nanospheres also have been investigated.[18] However, it is uncertain whether such a DNA-encoded method can be generally applied to control morphologies of anisotropic nanoparticles, especially AuNRs, whose plasmonic activity is highly dependent on their geometrical shape and size. Herein, we report a simple method

[*] T. Song, Dr. X. Wang, Prof. H. Liang
CAS Key Laboratory of Soft Matter Chemistry, Hefei National Laboratory for Physical Sciences at Microscale, Collaborative Innovation Center of Chemistry for Energy Materials (iChEM), University of Science and Technology of China
Hefei, Anhui 230026 (P. R. China)
E-mail: hjliang@ustc.edu.cn
T. Song, Dr. L. Tang, L. H. Tan, N. S. R. Satyavolu, Dr. H. Xing, Dr. Z. Wang, Prof. Y. Lu
Department of Chemistry, Department of Materials Science and Engineering, University of Illinois at Urbana-Champaign
Urbana, IL 61801 (USA)
E-mail: yi-lu@illinois.edu
Dr. L. Tang, Prof. J. Li
Department of Chemistry, Beijing Key Laboratory for Analytical Methods and Instrumentation, Key Laboratory of Bioorganic Phosphorus Chemistry & Chemical Biology, Tsinghua University
Beijing 100084 (P. R. China)

[**] This work was supported by the China Scholarship Council, the National Natural Science Foundation of China (21434007, 91427304, and 91127046), the National Basic Research Program of China (2012CB821500), and the US National Science Foundation (CMMI-0749028 to Y.L.).

Supporting information for this article is available on the WWW under http://dx.doi.org/10.1002/anie.201500838.

for tuning the plasmonic properties of the nanorods in a wide plasmonic range (550–1010 nm) by changing only the DNA sequence employed in the overgrowth. This is the first time that we demonstrated the use of modified DNA (phosphorothioate modifications) to achieve a broader scope of property tuning beyond what can be achieved by canonical bases (Figure 1 a).

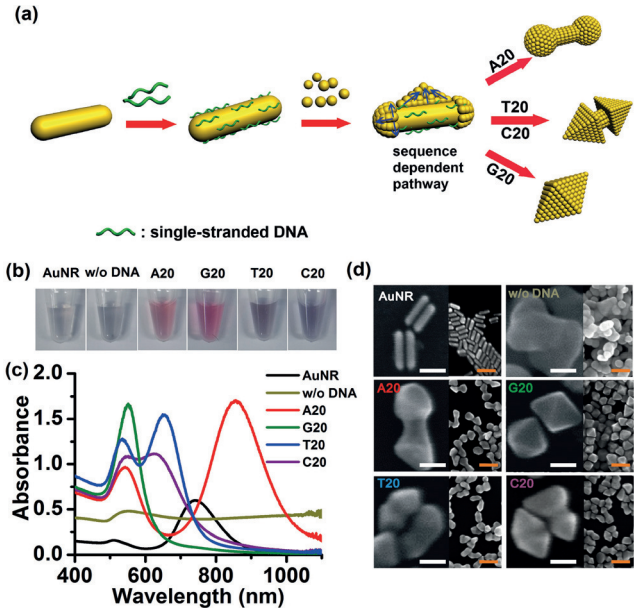

Figure 1. a) A proposed mechanism of overgrowth of AuNRs by homooligomeric DNA with different sequences. b) The color of the solution containing different nanoparticles, c) UV/Vis absorption spectra, and d) SEM images of AuNRs and their overgrowth in the absence of DNA (w/o DNA) or in the presence of A20, G20, T20, and C20.

The AuNR seeds were synthesized using a silver-ion-assisted method reported previously.[10a] The purified AuNRs displayed a light-brown color with transverse and longitudinal localized surface plasmon resonance (T-LSPR and L-LSPR) absorptions at 511 and 742 nm, and an average aspect ratio of 3.6 (length 58 ± 6 nm × width 16 ± 2 nm, Figure S1). To control the AuNR overgrowth using different DNA sequences, we first incubated the AuNR seed with a homooligomer of 20 adenine, guanine, cytosine, or thymine deoxyribonucleotides (called A20, G20, C20, and T20, respectively; Table S1) at room temperature. After incubation for one hour, the following solutions were then added in the following order: hydroxylamine (NH_2OH) as a mild reducing agent and hydrogen tetrachloroaurate as the gold precursor. These procedures resulted in different colored solutions and UV/Vis absorbance spectra for the different DNA sequences employed (Figure 1 b,c). In the absence of any DNA, the procedure led to visible sedimentation and aggregates, as shown by the disappearance of the plasmon resonance peaks and the appearance of a weak and broad T-LSPR peak at ca. 549 nm, which further indicated the formation of large clusters with irregular shapes and low stability.

In contrast, the nanoparticles obtained in the presence of DNA show high stability, yield, and reproducibility. Specifically, the presence of A20 transformed the solution from light brown to red (Figure 1 b), because the L-LSPR peak was red-shifted to 856 nm with a significant increase in intensity, accompanied by a slight red-shift of the T-LSPR peak to 543 nm (Figure 1 c). SEM images showed the formation of dumbbell-shaped nanostructures, with extension in length to 96 ± 6 nm (Figure 1 d). Interestingly, in the presence of G20, the solution turned magenta (Figure 1 b), as a result of two SPR peaks merged together at 551 nm (Figure 1 c). The SEM images showed that the AuNRs have evolved into octahedron nanoparticles, without significant variation in length (63 ± 4 nm). On the other hand, the presence of T20 (or C20) resulted in a purple solution, due to a blue-shift of the L-LSPR peak to 649 nm (or 624 nm) and a slight red-shift of the T-LSPR peak to 535 nm (or 545 nm; Figure 1 c). The particles with T20 or C20 grew into cracked octahedra with smooth facets,[17b] having an average length of 77 ± 8 nm and 71 ± 6 nm, respectively (Figures 1 b,d and S2). Despite having similar shapes between T20 and C20, the LSPR peaks are different due to the different gap distance between the two pointed ends (17 ± 3 nm for C20 and 24 ± 3 nm for T20).

To understand the sequence-dependent overgrowth of AuNRs in more detail, kinetic studies were performed (Figures 2, S3, and S4). We focused our study on A20 and G20, because the cracked-octahedron shape formed from T20 or C20 is a combination of the dumbbell obtained from A20- and the octahedron obtained from G20-encoded growth. In the presence of A20, the color of the growth solution gradually turned from light brown to red in ten minutes (Figure 2 a). The L-LSPR peak of the initial AuNRs at 742 nm not only red-shifted to 890 nm in five minutes, but also increased in intensity during the whole growth process. During the same period, the T-LSPR peak at 511 nm showed little red-shift (Figure 2 b).

The intermediates were obtained by quenching the reactions at different time points with excess mercaptopropionic acid and characterized by SEM. In the presence of A20, the terminals of the AuNPs grew larger than the middle regions forming dumbbell shape after five minutes (Figures 2 a,c and S4a). In contrast, in the presence of G20, the color changed from light brown to blue and then pink (Figure 2 d). The L-LSPR peak at 742 nm gradually blue-shifted to 591 nm, without significant change in intensity after two minutes, whereas the T-LSPR at 511 nm red-shifted to 542 nm. Eventually, the two SPR bands merged into a single peak at 551 nm (Figures 2 e and S3b). The SEM images showed an increase in the transverse growth of the nanorods during the whole process, finally yielding pointy termini (Figures 2 d,f and S4b).

To provide further insight into the mechanism of the sequence-dependent growth process, we performed statistical analyses on the dimensions of the nanoparticles during the overgrowth process (Figure 2 c,f). The length of nanoparticles is defined as the distance along the longitudinal direction, whereas the width is the diameter of the middle region. In the presence of A20, the AuNRs gradually extended their length from 58 ± 6 nm to 82 ± 6 nm in five minutes, corresponding to the continuous red-shifts of L-LSPR peaks in UV/Vis spectra within that period. No significant change of the width was

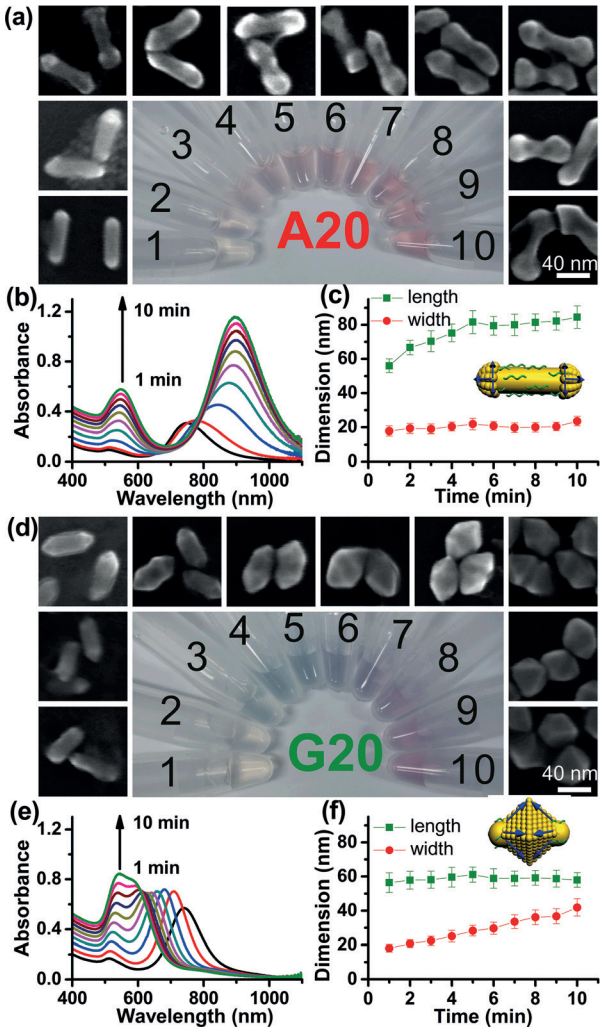

Figure 2. Kinetics of the nanoparticle growth process monitored by color changes, corresponding SEM micrographs, and UV/Vis absorption in the presence of A20 (a and b) and G20 (d and e). The statistical analyses on the dimensions of resulting nanoparticles encoded by A20 (c) and G20 (f).

observed within the first ten minutes (Figure 2c). In contrast, the G20-encoded process underwent little longitudinal growth, but a significant increase in width, from 16 ± 2 nm to 42 ± 5 nm in ten minutes (Figure 2f). Consequently, the aspect ratio decreased from 3.6 to 1.4, in agreement with the blue-shift of the L-LSPR peaks in the UV/Vis spectra. The kinetic studies on UV/Vis absorbance and SEM images of AuNR overgrowth caused by T20 and C20 suggest that the growth went through combinations of the previous two representative pathways (Figures S3c, S3d, S4c, and S4d). As such, the nanostructure grown from T20 or C20 result in the cracked octahedron which is a shape in between the nanodumbbell and nanooctahedron (Figure 1).

In understanding the mechanism, we noticed two interesting observations in the growth, 1) the growth all started from the ends of AuNRs, and 2) the stronger the binding affinity of DNA to the gold surface, the less the diameter grows. Based on these observations, we propose that the growth of nanoparticles initiates at the terminal parts of AuNRs, because of the high surface curvature and less dense DNA coating at the end facets of the rods.[19] The subsequent growth mode is dependent on the binding affinity between DNA with gold.[20] The higher energy facets on the surface of the AuNRs (i.e., the sides which are {110} and {100} facets) were stabilized by stronger binding affinity bases, and resulted in a less transverse growth of nanoparticles. (For more details on the mechanism refer to the Supporting Information)

In comparison to the previously reported templates for tuning the morphology of AuNRs,[11a,13] The DNA molecules exhibit superior control due to its sequence programmability. To maximize the programmability of DNA in encoding or controlling the shapes of nanoparticles, we employed mixed sequences with various base compositions, and applied them to modulate the overgrowth of nanorods (Figures 3 and S5).

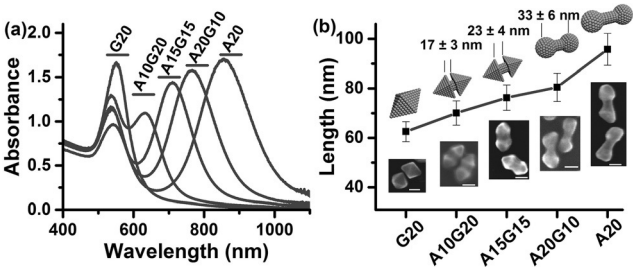

Figure 3. Morphological control of AuNR overgrowth using different DNA sequence combinations, monitored by UV/Vis absorption (a) and SEM (b). Scale bars = 20 nm.

Interestingly, when base A is combined with C, the final products are in dumbbell shape, similar to that of A alone (Figure S5a,b). Similarly, the combination of G and T resulted in the same octahedron shape as that in G alone (Figure S5c,d). These results indicate that base A and G have a dominating effect on the final morphology of nanoparticles when combined with base C or T, respectively. We then investigated the effect of combining the two dominating bases, A and G. As shown in Figure 3a, upon increasing A in the combination sequence, the L-LSPR peak red-shifted from 551 nm (displayed by the G20 alone) to 856 nm (displayed by A20 alone). Additionally, we noted that the nanoparticles synthesized with shorter DNA sequences (e.g., five bases) were less stable than those synthesized with longer DNA sequences, possibly due to a weaker stabilization with shorter strands. Therefore, strands longer than ten bases were typically used, but beyond a certain length that maintains such stability, the length of DNA play little role (Figure S6), except in the case of oligo C and and oligo G, which tend to form the i-motif and G-quadruplex, respectively. From the SEM images, we found that increasing the number of A bases in the combination sequence facilitated the growth of nanoparticles along the longitudinal direction (Figure 3b), resulting in shapes ranging from octahedron to cracked octahedron and finally dumbbell shape. The length of the gaps located in the middle of the nanoparticles changed from 17 ± 3 nm to 33 ± 6 nm as the consecutive A length increased from 10 to 20.

To further expand the versatility of DNA in controlling the geometric and plasmonic behavior of AuNPs, we inves-

tigated the effect of phosphorothioate (PS)-modified DNA,[21] on the morphology and plasmonic properties of the nanoparticles. Excitingly, we found that the L-LSPR peaks of resulting nanoparticles red-shifted dramatically from 856 to 1011 nm when more PS modifications are introduced into the A20 strands (Figure 4). Introduction of one, two, and four PS

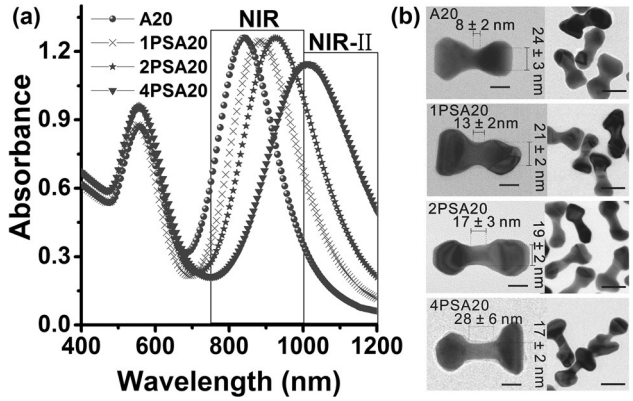

Figure 4. Tuning the plasmonic properties of the AuNRs with PS-modified DNA. a) The UV/Vis absorbance and b) TEM images of synthesized nanoparticles using A20 with different numbers of PS modification. Scale bars are 20 nm (left) and 50 nm (right).

modifications to the A20 strands (1PSA20, 2PSA20, 4PSA20) resulted in the L-LSPR peaks of the final product red-shifted by 40, 79, and 155 nm as compared to the DNA without PS modification (A20), with minimal shift of the T-LSPR peaks (Figure 4a). More importantly, the above method allowed tuning of the L-LSPR peaks of resulting nanoparticles into the second near-infrared[22] (NIR-II) region (1011 nm for 4PSA20 particles, Figures 4a and S7a). Interestingly, despite the very different L-LSPR peak positions, the resulting nanostructures were nanodumbbell shape, with almost the same length, irrespective of the number of PS modifications involved (Figures 4b, S7b, and S8). Instead, increasing the number of PS modifications induced larger intraparticle gaps and flattened ends, which could contribute to the red-shift in peaks.[23] In addition, the amount of growth on the sides of the nanoparticles was found to decrease from 21 ± 2 nm to 17 ± 2 nm, when the number of PS modifications increased from one to four in the A20 sequence. This is due to better stabilization of the {110} and {100} facets on the sides by the PS-modified DNA with higher binding affinity (Figures 4b and S7b).

To obtain further insight into this effect, we performed discrete dipole approximation (DDA) calculations using the DDSCAT program.[24] As shown in Figure S9, when the width of the middle regions of nanoparticles became smaller, the L-LSPR peaks further red-shifted. We proposed that the observed red-shifts in the PS modification systems are the results of both flattened ends and less growth in the middle region, probably induced by the increased binding affinity between the PS-modified DNA with AuNP.[25] The L-LSPR peak of the resulting nanoparticles is not only dominated by PS modification but also sequence-dependent. Using the T20 strands with four PS modifications, the L-LSPR peak of the resulting nanoparticles blue-shifted from 742 nm to 726 nm (Figure S10).

In conclusion, we have demonstrated the use of different DNA sequences to control the overgrowth of AuNRs with high yield and reproducibility, resulting in nanoparticles with diverse geometric and plasmonic properties. Detailed kinetic studies showed two representative pathways for the shape control, one influenced by the presence of A20 that promoted longitudinal growth, which finally evolved into dumbbell nanostructures, and the other by G20 that induced transverse growth, which resulted in octahedron shapes. A combination of the above two pathways can explain the growth and final shapes of nanoparticles encoded by T20 and C20. The programmability of the DNA to fine-tune the shapes and corresponding optical properties of the nanoparticles has further been validated by using different ratios of two-base combinations (e.g., AG) or PS modification, resulting in a tuning of the L-LSPR of the nanoparticles into the second near-infrared (NIR-II) region beyond 1000 nm. Achieving the ability to tune the absorbance into the NIR-II region is significant because it allows bioimaging with deeper penetration.[26] We believe that this growth method could tune the plasmonic properties even further if AuNR seeds of higher aspect ratios were used. In comparison with previous methods of tuning the L-LSPR of AuNRs into the NIR-II region, such as by replacing the bromide ions with iodide,[27] the method shown here produced nanoparticles with not only excellent plasmonic properties, but also DNA on the surface that allows biorecognition, with potential applications in nanoscale assemblies,[17a,28] sensing, and therapy.[29]

Keywords: DNA · gold · nanoparticles · nanostructures · surface plasmon resonance

How to cite: *Angew. Chem. Int. Ed.* **2015**, *54*, 8114–8118
Angew. Chem. **2015**, *127*, 8232–8236

[1] a) L. J. Sherry, S.-H. Chang, G. C. Schatz, R. P. Van Duyne, B. J. Wiley, Y. Xia, *Nano Lett.* **2005**, *5*, 2034–2038; b) X. Huang, S. Neretina, M. A. El-Sayed, *Adv. Mater.* **2009**, *21*, 4880–4910; c) N. J. Halas, S. Lal, W.-S. Chang, S. Link, P. Nordlander, *Chem. Rev.* **2011**, *111*, 3913–3961.

[2] H. Chen, L. Shao, Q. Li, J. Wang, *Chem. Soc. Rev.* **2013**, *42*, 2679–2724.

[3] a) J. Liu, M. Yu, X. Ning, C. Zhou, S. Yang, J. Zheng, *Angew. Chem. Int. Ed.* **2013**, *52*, 12572–12576; *Angew. Chem.* **2013**, *125*, 12804–12808; b) J. Liu, M. Yu, C. Zhou, S. Yang, X. Ning, J. Zheng, *J. Am. Chem. Soc.* **2013**, *135*, 4978–4981.

[4] J. S. DuChene, B. C. Sweeny, A. C. Johnston-Peck, D. Su, E. A. Stach, W. D. Wei, *Angew. Chem. Int. Ed.* **2014**, *53*, 7887–7891; *Angew. Chem.* **2014**, *126*, 8021–8025.

[5] T. Zhang, H. Zhao, S. He, K. Liu, H. Liu, Y. Yin, C. Gao, *ACS Nano* **2014**, *8*, 7297–7304.

[6] L. Vigderman, B. P. Khanal, E. R. Zubarev, *Adv. Mater.* **2012**, *24*, 4811–4841.

[7] M. R. K. Ali, S. R. Panikkanvalappil, M. A. El-Sayed, *J. Am. Chem. Soc.* **2014**, *136*, 4464–4467.

[8] B. Nikoobakht, M. A. El-Sayed, *Chem. Mater.* **2003**, *15*, 1957–1962.

[9] a) G. S. Terentyuk, G. N. Maslyakova, L. V. Suleymanova, N. G. Khlebtsov, B. N. Khlebtsov, G. G. Akchurin, I. L. Maksimova,

V. V. Tuchin, *J. Biomed. Opt.* **2009**, *14*, 021016; b) L. Dykman, N. Khlebtsov, *Chem. Soc. Rev.* **2012**, *41*, 2256 – 2282.
[10] a) A. M. Alkilany, P. K. Nagaria, M. D. Wyatt, C. J. Murphy, *Langmuir* **2010**, *26*, 9328 – 9333; b) C. Gao, Q. Zhang, Z. Lu, Y. Yin, *J. Am. Chem. Soc.* **2011**, *133*, 19706 – 19709; c) J. S. DuChene, W. Niu, J. M. Abendroth, Q. Sun, W. Zhao, F. Huo, W. D. Wei, *Chem. Mater.* **2013**, *25*, 1392 – 1399; d) L. Vigderman, E. R. Zubarev, *Chem. Mater.* **2013**, *25*, 1450 – 1457.
[11] a) E. Carbó-Argibay, B. Rodríguez-González, J. Pacifico, I. Pastoriza-Santos, J. Pérez-Juste, L. M. Liz-Marzán, *Angew. Chem. Int. Ed.* **2007**, *46*, 8983 – 8987; *Angew. Chem.* **2007**, *119*, 9141 – 9145; b) C.-K. Tsung, X. Kou, Q. Shi, J. Zhang, M. H. Yeung, J. Wang, G. D. Stucky, *J. Am. Chem. Soc.* **2006**, *128*, 5352 – 5353.
[12] K. Sohn, F. Kim, K. C. Pradel, J. Wu, Y. Peng, F. Zhou, J. Huang, *ACS Nano* **2009**, *3*, 2191 – 2198.
[13] X. Kou, S. Zhang, Z. Yang, C.-K. Tsung, G. D. Stucky, L. Sun, J. Wang, C. Yan, *J. Am. Chem. Soc.* **2007**, *129*, 6402 – 6404.
[14] a) A. Udomprasert, M. N. Bongiovanni, R. Sha, W. B. Sherman, T. Wang, P. S. Arora, J. W. Canary, S. L. Gras, N. C. Seeman, *Nature Nanotech.* **2014**, *9*, 537 – 541; b) D. A. Rusling, A. R. Chandrasekaran, Y. P. Ohayon, T. Brown, K. R. Fox, R. Sha, C. Mao, N. C. Seeman, *Angew. Chem. Int. Ed.* **2014**, *53*, 3979 – 3982; *Angew. Chem.* **2014**, *126*, 4060 – 4063; c) F. Zhang, J. Nangreave, Y. Liu, H. Yan, *J. Am. Chem. Soc.* **2014**, *136*, 11198 – 11211; d) J. Fu, Y. R. Yang, A. Johnson-Buck, M. Liu, Y. Liu, N. G. Walter, N. W. Woodbury, H. Yan, *Nat. Nanotechnol.* **2014**, *9*, 531 – 536.
[15] a) J. H. Lee, D. P. Wernette, M. V. Yigit, J. Liu, Z. Wang, Y. Lu, *Angew. Chem. Int. Ed.* **2007**, *46*, 9006 – 9010; *Angew. Chem.* **2007**, *119*, 9164 – 9168; b) J. H. Lee, N. Y. Wong, L. H. Tan, Z. Wang, Y. Lu, *J. Am. Chem. Soc.* **2010**, *132*, 8906 – 8908.
[16] a) A. P. Alivisatos, K. P. Johnsson, X. G. Peng, T. E. Wilson, C. J. Loweth, M. P. Bruchez, P. G. Schultz, *Nature* **1996**, *382*, 609 – 611; b) C. A. Mirkin, R. L. Letsinger, R. C. Mucic, J. J. Storhoff, *Nature* **1996**, *382*, 607 – 609; c) W. Cheng, M. J. Campolongo, J. J. Cha, S. J. Tan, C. C. Umbach, D. A. Muller, D. Luo, *Nat. Mater.* **2009**, *8*, 519 – 525; d) Y. Xiang, Y. Lu, *Nat. Chem.* **2011**, *3*, 697 – 703; e) T. Song, H. Liang, *J. Am. Chem. Soc.* **2012**, *134*, 10803 – 10806; f) X. Xie, W. Xu, X. Liu, *Acc. Chem. Res.* **2012**, *45*, 1511 – 1520; g) T. Song, S. Xiao, D. Yao, F. Huang, M. Hu, H. Liang, *Adv. Mater.* **2014**, *26*, 6181 – 6185; h) S. J. Tan, J. S. Kahn, T. L. Derrien, M. J. Campolongo, M. Zhao, D.-M. Smilgies, D. Luo, *Angew. Chem. Int. Ed.* **2014**, *53*, 1316 – 1319; *Angew. Chem.* **2014**, *126*, 1340 – 1343.
[17] a) Z. Wang, J. Zhang, J. M. Ekman, P. J. A. Kenis, Y. Lu, *Nano Lett.* **2010**, *10*, 1886 – 1891; b) Z. Wang, L. Tang, L. H. Tan, J. Li, Y. Lu, *Angew. Chem. Int. Ed.* **2012**, *51*, 9078 – 9082; *Angew. Chem.* **2012**, *124*, 9212 – 9216; c) J. Wu, L. H. Tan, K. Hwang, H. Xing, P. Wu, W. Li, Y. Lu, *J. Am. Chem. Soc.* **2014**, *136*, 15195 – 15202; d) L. H. Tan, H. Xing, Y. Lu, *Acc. Chem. Res.* **2014**, *47*, 1881 – 1890.
[18] J. Shen, L. Xu, C. Wang, H. Pei, R. Tai, S. Song, Q. Huang, C. Fan, G. Chen, *Angew. Chem. Int. Ed.* **2014**, *53*, 8338 – 8342; *Angew. Chem.* **2014**, *126*, 8478 – 8482.
[19] R. Costi, A. E. Saunders, U. Banin, *Angew. Chem. Int. Ed.* **2010**, *49*, 4878 – 4897; *Angew. Chem.* **2010**, *122*, 4996 – 5016.
[20] H. Kimura-Suda, D. Y. Petrovykh, M. J. Tarlov, L. J. Whitman, *J. Am. Chem. Soc.* **2003**, *125*, 9014 – 9015.
[21] T. J. Bandy, A. Brewer, J. R. Burns, G. Marth, T. Nguyen, E. Stulz, *Chem. Soc. Rev.* **2011**, *40*, 138 – 148.
[22] G. Hong, et al., *Nat. Commun.* **2014**, *5*, 4206.
[23] V. Myroshnychenko, J. Rodriguez-Fernandez, I. Pastoriza-Santos, A. M. Funston, C. Novo, P. Mulvaney, L. M. Liz-Marzan, F. J. Garcia de Abajo, *Chem. Soc. Rev.* **2008**, *37*, 1792 – 1805.
[24] B. T. Draine, P. J. Flatau, *J. Opt. Soc. Am. A* **1994**, *11*, 1491 – 1499.
[25] W. Zhou, F. Wang, J. Ding, J. Liu, *ACS Appl. Mater. Interfaces* **2014**, *6*, 14795 – 14800.
[26] A. M. Smith, M. C. Mancini, S. Nie, *Nat. Nanotechnol.* **2009**, *4*, 710 – 711.
[27] M. Grzelczak, A. Sánchez-Iglesias, B. Rodríguez-González, R. Alvarez-Puebla, J. Pérez-Juste, L. M. Liz-Marzán, *Adv. Funct. Mater.* **2008**, *18*, 3780 – 3786.
[28] A. J. Senesi, D. J. Eichelsdoerfer, R. J. Macfarlane, M. R. Jones, E. Auyeung, B. Lee, C. A. Mirkin, *Angew. Chem. Int. Ed.* **2013**, *52*, 6624 – 6628; *Angew. Chem.* **2013**, *125*, 6756 – 6760.
[29] a) A. Kuzyk, R. Schreiber, H. Zhang, A. O. Govorov, T. Liedl, N. Liu, *Nat. Mater.* **2014**, *13*, 862 – 866; b) X. Yang, X. Liu, Z. Liu, F. Pu, J. Ren, X. Qu, *Adv. Mater.* **2012**, *24*, 2890 – 2895.

Received: January 28, 2015
Revised: April 3, 2015
Published online: June 10, 2015

